THE JOURNAL OF BIOLOGICAL CHEMISTRY VOL. 291, NO. 4, pp. 1591–1603, January 22, 2016

Mitochondrial Translocator Protein (TSPO) Function Is Not Essential for Heme Biosynthesis*

Received for publication, August 17, 2015, and in revised form, November 30, 2015 Published, JBC Papers in Press, December 1, 2015, DOI 10.1074/jbc.M115.686360

Amy H. Zhao[‡], Lan N. Tu[‡], Chinatsu Mukai[§], Madhu P. Sirivelu[¶], Viju V. Pillai[‡], Kanako Morohaku[‡], Roy Cohen[§], and Vimal Selvaraj[‡1]

From the [‡]Department of Animal Science, College of Agriculture and Life Sciences, Cornell University, Ithaca, New York 14853, the [§]Baker Institute for Animal Health, College of Veterinary Medicine, Cornell University, Ithaca, New York 14853, and the [¶]Department of Clinical Pathology, College of Veterinary Medicine, University of Pennsylvania, Philadelphia, Pennsylvania 19104

Function of the mammalian translocator protein (TSPO; previously known as the peripheral benzodiazepine receptor) remains unclear because its presumed role in steroidogenesis and mitochondrial permeability transition established using pharmacological methods has been refuted in recent genetic studies. Protoporphyrin IX (PPIX) is considered a conserved endogenous ligand for TSPO. In bacteria, TSPO was identified to regulate tetrapyrrole metabolism and chemical catalysis of PPIX in the presence of light, and in vertebrates, TSPO function has been linked to porphyrin transport and heme biosynthesis. Positive correlation between high TSPO expression in cancer cells and susceptibility to photodynamic therapy based on their increased ability to convert the precursor 5-aminolevulinic acid (ALA) to PPIX appeared to reinforce this mechanism. In this study, we used TSPO knock-out (*Tspo*$^{-/-}$) mice, primary cells, and different tumor cell lines to examine the role of TSPO in erythropoiesis, heme levels, PPIX biosynthesis, phototoxic cell death, and mitochondrial bioenergetic homeostasis. In contrast to expectations, our results demonstrate that TSPO deficiency does not adversely affect erythropoiesis, heme biosynthesis, bioconversion of ALA to PPIX, and porphyrin-mediated phototoxic cell death. TSPO expression levels in cancer cells do not correlate with their ability to convert ALA to PPIX. In fibroblasts, we observed that TSPO deficiency decreased the oxygen consumption rate and mitochondrial membrane potential ($\Delta\Psi$m) indicative of a cellular metabolic shift, without a negative impact on porphyrin biosynthetic capability. Based on these findings, we conclude that mammalian TSPO does not have a critical physiological function related to PPIX and heme biosynthesis.

Mammalian translocator protein (TSPO),[2] previously known as the peripheral benzodiazepine receptor (1), is a highly conserved protein enriched in the outer mitochondrial membrane (2). Despite extensive efforts to characterize TSPO, its precise physiological function remains elusive (3, 4). High levels of TSPO expression in steroidogenic cells, its localization to the outer mitochondrial membrane, and increased steroid production upon pharmacological binding led to the primary prospective model that TSPO was a mitochondrial cholesterol transporter essential for steroidogenesis (5). In recent studies using precise genetic tools, we and others have systematically refuted the involvement of TSPO in this process (6–10). Similarly, copurification of TSPO with putative members of the mitochondrial permeability transition pore (MPTP) (11) and effects mediated by TSPO binding drugs on modulating apoptosis (12, 13) resulted in a secondary model that TSPO was associated with MPTP function and cell death (14). Again, recent discovery of the molecular identity of MPTP (15) and direct testing of MPTP function in the absence of TSPO (16) disputed its direct involvement in cell death processes (reviewed in Ref. 4). These new developments have shifted focus of TSPO function to yet another molecule considered to be an endogenous ligand, protoporphyrin IX (PPIX) (17).

Binding of porphyrins to TSPO has been a consistent property reported in bacteria (18), plants (19), and animals (17). In *Rhodobacter sphaeroides*, TSPO was found localized to the outer membrane (18) and played a role in negatively regulating photosynthesis genes in response to oxygen (20). Examining tetrapyrrole metabolism after providing the precursor ALA to different *Tspo* mutants of *R. sphaeroides* led to a conclusion that TSPO facilitated the export of excessive intermediates in the tetrapyrrole pathway (21). In *Bacillus cereus*, TSPO mediated a light-induced degradation of PPIX (22). In *Arabidopsis thaliana*, it was observed that TSPO attenuated ALA-induced porphyria through a potential scavenging mechanism (23). In *Danio rerio* embryos, pharmacological binding of TSPO protein using PK11195 (*N*-butan-2-yl-1-(2-chlorophenyl)-*N*-methylisoquinoline-3-carboxamide) or morpholino antisense oligonucleotides resulted in a loss of circulating erythrocytes

* This work was supported by funds from the Cornell College of Agriculture and Life Sciences (startup funds to V. S.); the Jane E Brody undergraduate research award and the Dextra undergraduate research endowment fund (to A. H. Z.); and fellowships from the Vietnam Education Foundation and the Cornell Center for Vertebrate Genomics (to L. N. T.). The authors declare that they have no conflicts of interest with the contents of this article.

[1] To whom correspondence should be addressed: Dept. of Animal Science, 204 Morrison Hall, 507 Tower Rd., Cornell University, Ithaca, NY 14853. Tel.: 607-255-6138; Fax: 607-255-9829; E-mail: vs88@cornell.edu.

[2] The abbreviations used are: TSPO, translocator protein; PPIX, protoporphyrin IX; PDT, photodynamic therapy; ALA, 5-aminolevulinic acid; MPTP, mitochondrial permeability transition pore; OCR, oxygen consumption rate; PK11195, *N*-butan-2-yl-1-(2-chlorophenyl)-*N*-methylisoquinoline-3-carboxamide; *Alas*, ALA synthase; *Alad*, ALA dehydratase; *Hmbs*, hydroxymethylbilane synthase; *Uros*, uroporphyrinogen III synthase; *Urod*, uroporphyrinogen decarboxylase; *Cpox*, coproporphyrinogen oxidase; *Ppox*, protoporphyrinogen oxidase; *Fech*, ferrochelatase; FCCP, carbonyl cyanide 4-(trifluoromethoxy) phenylhydrazone; TMRM, tetramethylrhodamine methyl ester.

(24). In *Gallus gallus*, pharmacological binding of TSPO using PK11195 decreased globin levels indicating a function in the regulation of heme availability for the assembly of functional hemoglobin (25).

Early studies using TSPO-binding drugs have suggested a functional link between mammalian (*Mus musculus* and *Homo sapiens*) TSPO and the induction of hemoglobin synthesis (26, 27). Subsequent studies identified that TSPO could bind the heme precursor PPIX with nanomolar affinity (17) and that TSPO induction that was concomitant with heme biosynthetic enzymes, suggesting a possible involvement in porphyrin transport important for heme biosynthesis (28, 29). It was also demonstrated that knockdown of TSPO expression resulted in mitochondrial accumulation of exogenous PPIX, suggesting that TSPO could be involved in heme metabolism (30).

Pathological overexpression of TSPO has been reported in several cancers like colon, breast, and skin cancers (31, 32). A strong correlation between the aggressive cancer phenotype and expression levels of TSPO has been established in several studies (33–35). Cancer cells also show an increased ability to produce endogenous PPIX when supplemented with ALA (36, 37), a photosensitization mechanism that forms the basis of porphyrin-mediated PDT. In this context, experiments have suggested that TSPO plays a major role in PDT by its action on porphyrins (38, 39).

In search of a functional basis for this proposed relationship between mammalian TSPO and PPIX, we use genetic models, *Tspo* gene deleted ($Tspo^{-/-}$) mice, $Tspo^{-/-}$ primary cells, and $Tspo^{\Delta/\Delta}$ cancer cells to investigate TSPO-specific actions. Our results demonstrate that TSPO is not essential for porphyrin and heme biosynthesis or porphyrin-mediated phototoxic cell death, but that TSPO deficiency affects mitochondrial energy homeostasis that may impact multiple cellular events and responses.

Experimental Procedures

$Tspo^{-/-}$ Mice—Generation and validation of $Tspo^{-/-}$ mice has been previously described (7). Animals were maintained in accordance with the National Institutes of Health Guide for the Care and Use of Laboratory Animals, and the Institutional Animal Care and Use Committee of Cornell University approved all procedures.

Cells—All cell culture procedures were performed at 37 °C under 5% CO_2. Primary murine fibroblasts were cultured from day 14 embryos in growth medium (DMEM containing 10% FBS and 1% nonessential amino acids). In brief, embryos were aseptically collected, and carcasses were minced and plated in cell culture dishes for attachment and growth. The cells were passaged once and frozen for use in experiments. Generation and culture of TSPO deleted MA-10 cells (MA-10:$Tspo^{\Delta/\Delta}$ cells) has been previously described (8). Human colon cancer cell lines were obtained from ATCC and cultured using recommended methods. Cell lines HCT116 and HT29 were cultured in McCoy's 5A medium containing 10% FBS. Cell line LOVO was cultured in F12K medium containing 10% FBS. Cell line DLD-1 was cultured in RPMI1640 containing 10% FBS.

Hematology and Bone Marrow Histology—Blood was collected in heparinized tubes (BD Biosciences). Erythrocyte counts, platelet, hematocrit, mean corpuscular volume, mean corpuscular hemoglobin, and mean corpuscular hemoglobin concentration were obtained using an automated analyzer (Advia 120, Siemens). Erythrocyte counts were also confirmed manually using a hemocytometer. Femurs were processed for histology by fixation in 10% formaldehyde, followed by slow decalcification and paraffin embedding. Thin 4-μm sections were cut and stained using hematoxylin and eosin. Bone marrow cytology was assessed on brush preparations made from the marrow and stained using modified Wright's stain. Marrow hematopoietic cellularity and percentage of erythroid cells were assessed on bone marrow histology and cytology preparations by a board certified veterinary pathologist, and the percentage of erythroid precursors was calculated. Images were captured under a light microscope (DM1000; Leica) using a color camera (ICC 50HD; Leica).

Measurement of Heme in Tissues—Heme content was determined using a fluorometric method as described (40). Liver, spleen, and bone marrow samples were homogenized in 1% Triton X-100 in Tris-buffered saline. Homogenized samples were centrifuged at 5000 $\times$ *g* for 10 min. 1 μl of the homogenate was added to 500 μl of saturated (2 M) oxalic acid and boiled for 30 min to produce PPIX from heme. Samples were then centrifuged at 10,000 $\times$ *g* for 10 min at 4 °C, and PPIX fluorescence in the supernatant was measured using a fluorescence spectrophotometer (Infinite 200; Tecan), under excitation at 400 nm and emission at 660 nm, and concentrations were calculated using a standard curve. Pre-existing non-heme PPIX was subtracted from total heme by using a duplicate, unboiled sample. Heme values were normalized to protein content in each sample.

PPIX Uptake and Phototoxicity—For estimating PPIX uptake, fibroblasts treated with 0 (control), 0.5, 1, or 1.5 μM PPIX (Sigma) for 4 h in serum-free medium were collected by trypsinization. The trypsin was neutralized using 0.7 mg/ml type II-O trypsin inhibitor (Sigma) in DMEM to avoid exposure to serum. Cells were then resuspended, fixed using 1% formaldehyde, and assayed using a flow cytometer at an excitation of 488 nm and an emission range of 620–630 nm (Gallios; Beckman Coulter) to estimate the median PPIX uptake by individual cells. For evaluating phototoxicity, fibroblasts were treated with PPIX (0 (control), 0.5, 1, or 1.5 μM) for 4 h as described above were exposed to light at 450 ($\pm$ 60)-nm wavelength at 160, 240, or 320 mJ using an 800 milliwatt mercury lamp light path fitted with a band-pass filter and a neutral density filter (OD 1.0). After exposure, fibroblasts were provided with growth medium and incubated for 6 h before labeling using propidium iodide (20 μg/ml) and Hoescht 33342 (1 μg/ml) to determine live and dead cells. Populations were counted after acquiring images with an inverted epifluorescence microscope (DM3000; Leica) using a monochromatic cooled camera (DFC365FX; Leica).

Bioconversion of ALA to PPIX—For *in vivo* experiments, ALA (25 mg/ml in PBS; Sigma) was administered to mice (250 mg/kg body weight intraperitoneal) and euthanized at 0 (baseline), 1, 4, or 8 h after ALA administration. Plasma, bone marrow (femurs), livers, and spleens were collected for estimating PPIX concentrations. For estimation of PPIX, samples were extracted using 1:1 methanol-1N perchloric acid (MeOH-PCA) on ice for

10 min, and the lysates were cleared by centrifugation at 10,000 × *g* for 10 min at 4 °C. Supernatants (100 μl) for each sample were analyzed for PPIX in black 96-well plates using a fluorescence spectrophotometer as described for heme, and concentrations were calculated using a standard curve. For plasma, data were represented as PPIX concentration per milliliter. For tissues, acidic pellets were neutralized with 1.5 M Tris acetate buffer and used to measure protein content using the bicinchoninic acid assay; PPIX concentrations were normalized to protein content. In a separate experiment, at 1 h after ALA administration, bone marrow (femurs) were collected for RNA extraction and quantitative PCR as described below.

For *in vitro* experiments, fibroblasts (density of 2,500 cells/cm^2), MA-10 cells (5,000 cells/cm^2), and colon cancer cell lines (5,000 cells/cm^2) were treated with 1 mM of ALA and incubated for baseline and 24 h. After incubation, cells were collected by trypsinization followed by neutralization using trypsin inhibitor in DMEM. Cells were lysed in 1:1 MeOH-PCA, and PPIX fluorescence was estimated as described above for tissue samples.

Western Blots—Samples were processed in Laemmli sample buffer as previously described (41), and protein concentrations were determined using a bichionic acid assay. Equal amounts of protein (25–50 μg/sample) were separated by SDS-PAGE and transferred to PVDF membranes. Membranes were then blocked using 5% nonfat dry milk in Tris-buffered saline containing 0.2% Tween 20. Incubations were carried out using a rabbit anti-TSPO monoclonal antibody (Abcam), a rabbit anti-IDH2 monoclonal antibody (Abcam), or a mouse anti-VDAC1 monoclonal antibody (Abcam) and a control mouse anti-actin monoclonal antibody (Li-Cor). Fluorescent IRDye800 goat anti-rabbit IgG and IRDye680 goat anti-mouse IgG were used for fluorescent labeling; membranes were imaged using a laser fluorescence scanner (Odyssey; Li-Cor).

PPIX and Mitochondrial Colocalization—Fibroblasts cultured in glass-bottomed 35-mm dishes (MatTek corporation) were treated with 1 μM PPIX in serum-free medium for 4 h. MitoTracker Green (Life Technologies) was added to label the mitochondria in live cells for the final 30 min of this incubation. Labeled cells were then provided with fresh medium, and high resolution images were acquired using a confocal microscope (Meta 510; Zeiss). Image analyses for colocalization of PPIX and MitoTracker were performed using the intensity correlation plugin in ImageJ (National Institutes of Health) (42) and calculating the Mander's overlap coefficient and Pearson's coefficient. At least 40 cells for each genotype were imaged and analyzed.

Quantitative PCR—Gene expression analyses using quantitative PCR were performed for both *in vitro* (fibroblasts and MA-10 cells) and *in vivo* (bone marrow) samples. Total RNA was extracted using TRIzol reagent (Life Technologies); reverse transcription of 1.5 μg of total RNA was performed using Multiscribe reverse transcriptase (Life Technologies). Gene expression assays for the different samples were performed using SYBR-green using intron-spanning primers for ALA synthase (*Alas*: 5′-TGTCGGTCTGGTGCAGTAATG-3′ and 5′-GGCATCATCTTAGCCAGGGT-3′), ALA dehydratase (*Alad*: 5′-GTTCTGCACAGCGGCTACTT-3′ and 5′-AGCTGGTTTACGCCATACCTG-3′), hydroxymethylbilane synthase (*Hmbs*: 5′-ATGAGGGTGATTCGAGTGGG-3′ and 5′-TTGTCTCCCGTGGTGGACATA-3′), uroporphyrinogen III synthase (*Uros*: 5′-CCAGCATCACGTTTTTCAGTCC-3′ and 5′-GTACTGGGGCCAATGGCTAT-3′), uroporphyrinogen decarboxylase (*Urod*: 5′-GGGTTCGGACTCCAGAATTTC-3′ and 5′-CCTGTCTCATGCACCAAACG-3′), coproporphyrinogen oxidase (*Cpox*: 5′-GCCATTTACTGCTATGGGTGT and 5′-AGCTTCCTTTAGAGTACGGTGG-3′), protoporphyrinogen oxidase (*Ppox*: 5′-ATGGGCCGGACTGTGATAGTA-3′ and 5′-CTTGCTGCCCTCCACTAAGA-3′), ferrochelatase (*Fech:* 5′-CAGACAGATGAGGCTATCAAAGG-3′ and 5′-CACAGCTTGTTGGACTGGATG-3′), and *Tspo* (5′-TGGGTGCCTTCACTCTGG-3′ and 5′-AATCACCATGCCTGAATCCT-3′). Samples were analyzed after normalization to the expression of glyceraldehyde-3-phosphate dehydrogenase (*Gapdh*: 5′-GCCTTCCGTGTTCCTACC-3′ and 5′-GCCTGCTTCACCACCTTC-3′) or TATA box binding protein (*Tbp*: 5′-CCTTGTACCCTTCACCAATGAC-3′ and 5′-ACAGCCAAGATTCACGGTAGA-3′). Relative quantifications of fold change were performed comparing *Ct* values from individual samples by applying the $2^{-\Delta\Delta Ct}$ method (43). Because of difficulty in designing intron-spanning primers, translocator protein 2 (*Tspo2*) expression was quantified using a TaqMan probe (Mm01281420_m1) with normalization to *Gapdh* (4352339E) (Life Technologies).

Adenoviral Expression of TSPO2—Adenoviruses that express TSPO2 were generated using the AdEasy system (44). In brief, *Tspo2* cDNA was cloned from a bone marrow sample into a shuttle vector (pAd-CMV), linearized using PacI, and transformed into AdEasier bacteria containing the adenoviral backbone plasmid (pAdEasy-1). Adenoviruses were packaged by transfection into HEK-293A cells and amplified for two cycles in the same cell line. Titers were estimated by quantifying viral DNA, and infection rates were assessed by *Tspo2* mRNA expression in the target cells by quantitative PCR. Control adenoviruses expressing *tdTomato* (Vector Biolabs) were amplified in HEK-293A cells and used as matched titers. Fibroblasts infected with adenoviral *Tspo2* or *tdTomato* were used after 48 h for experiments evaluating the bioconversion of ALA to PPIX as described above.

Oxygen Consumption Rate—For measurements of mitochondrial respiration, oxygen consumption rates (OCR) were measured using an XF24 Extracellular Flux Analyzer (Seahorse Bioscience). Fibroblasts ($Tspo^{fl/fl}$ and $Tspo^{-/-}$) were plated at a density of 30,000 cells in the XF24 cell culture microplates in regular culture medium (10% FBS, 25 mM glucose, 1 mM pyruvate) overnight. One hour before assay, cells were washed and incubated in XF assay medium (no bicarbonate) supplemented with 25 mM glucose and 1 mM pyruvate at 37 °C in a CO_2-free atmosphere. OCR was measured real time every 3–5 min. Oligomycin, carbonyl cyanide 4-(trifluoromethoxy)phenylhydrazone (FCCP), antimycin A, and rotenone were sequentially injected into each well to assess basal respiration, coupling of respiratory chain, proton leak, and mitochondrial spare respiratory capacity.

Mitochondrial Volume, Mass, and Membrane Potential—Fibroblasts, *Tspo*$^{fl/fl}$ and *Tspo*$^{-/-}$, were seeded on 35-mm glass-bottomed dishes (MatTek) overnight in high glucose DMEM, 10% FBS. Cells were stained with 100 nM MitoTracker Green FM at 37 °C for 1 h in the dark, washed with PBS, and changed to phenol red-free high glucose DMEM, 10% FBS, 10 mM HEPES for live cell imaging using Zeiss LSM 510 confocal microscopy. Images were collected as z-stacks and analyzed for volume after adjustment of threshold using three-dimensional Manager plugin in ImageJ (45).

For mitochondrial membrane potential measurement, cells were costained with 100 nM MitoTracker Green FM and 20 nM tetramethylrhodamine methyl ester (TMRM) and imaged as above or intensities measured using a flow cytometer (Gallios; Beckman Coulter). After baseline values were taken, the cells were incubated with 5 μM oligomycin at 37 °C for 30 min before imaging. Depolarization was then induced by 10 μM FCCP, and images were taken after 2 min. Intensities of TMRM were normalized to those of MitoTracker Green for comparisons of $\Delta\psi$m between the two genotypes. Mitochondrial masses were assessed by comparing the intensities of MitoTracker green and were also confirmed by estimating the amounts of mitochondrial proteins IDH2 and VDAC1 using Western blots (as described above).

PK11195 Treatments—For ALA to PPIX bioconversion, fibroblasts were treated with PK11195 (1 μM) in 0.1% DMSO (control) in medium containing 1 mM of ALA and incubated for 24 h. After incubation, cells were collected and lysed, and PPIX fluorescence was estimated as described above. For measuring $\Delta\psi$m, fibroblasts treated with PK11195 (0 and 100 nM and 1 μM) were incubated for 60 min and stained with MitoTracker Green FM and TMRM, and intensities were measured using flow cytometry as described above.

Statistics—The responses measured for two experimental groups were compared using Student's *t* test; comparisons for more than two groups were performed using analysis of variance and post hoc Tukey's test ($p < 0.05$ was considered significant). All analyses were performed using Prism5 (GraphPad), and the data are represented as means ± S.E. of the mean.

TABLE 1

Erythrocyte characteristics in *Tspo*$^{-/-}$ mice

MCV, mean corpuscular volume; MCH, mean corpuscular hemoglobin; MCHC, mean corpuscular hemoglobin concentration; CHCM, cell hemoglobin concentration mean; RDW, red blood cell distribution width.

Parameters	TSPO$^{fl/fl}$	TSPO$^{-/-}$	*p* value
Erythrocytes (10^6 cells/μl)	9.8 ± 0.05	9.8 ± 0.15	1.0000
Platelets ($10^3/\mu$l)	1284.4 ± 182.24	1508.6 ± 196.58	0.4272
Hemoglobin (g/dL)	15.7 ± 0.15	15.8 ± 0.16	0.5028
Hematocrit (%)	52.8 ± 0.66	52.0 ± 0.44	0.3466
MCV (fL)	54.20 ± 0.8	53.00 ± 1.09	0.4021
MCH (pg)	15.6 ± 0.24	16.0 ± 0.31	0.3466
MCHC (g/dL)	29.0 ± 0.00	30.0 ± 0.31	0.3411
CHCM (g/dL)	27.0 ± 0.00	27.4 ± 0.24	0.1411
RDW (%)	12.6 ± 0.24	12.4 ± 0.25	0.5796

Results

Erythropoiesis Is Not Affected in Tspo$^{-/-}$ *Mice*—Blood collected from *Tspo*$^{-/-}$ mice showed that all their erythrocyte/hemoglobin parameters were within physiological intervals and were not different from *Tspo*$^{fl/fl}$ mice (Table 1). Bone marrow from both *Tspo*$^{fl/fl}$ and *Tspo*$^{-/-}$ mice exhibited identical morphological features and cellular composition after hematoxylin and eosin staining (Fig. 1*A*). Percentages of bone marrow erythroid cells were not different between *Tspo*$^{fl/fl}$ and *Tspo*$^{-/-}$ mice (Fig. 1*B*). Hematology analyses showed no significant differences between *Tspo*$^{fl/fl}$ and *Tspo*$^{-/-}$ mice (Table 1), and values were within physiological intervals observed for C57BL/6 mice. Measurements that indicated hemoglobin concentration also showed no differences between *Tspo*$^{fl/fl}$ and *Tspo*$^{-/-}$ mice. Bone marrow gene expression of enzymes involved in PPIX biosynthesis showed some differences between *Tspo*$^{fl/fl}$ and *Tspo*$^{-/-}$ mice (Fig. 2). No significant changes were observed for *Hmbs*, *Uros*, *Urod*, and *Ppox* expression. Baseline expression of *Fech* was significantly higher in *Tspo*$^{-/-}$ compared with *Tspo*$^{fl/fl}$ bone marrow, but expression of *Fech* and *Alas* was significantly down-regulated to similar levels after ALA treatment in both *Tspo*$^{fl/fl}$ and *Tspo*$^{-/-}$ bone marrow. In *Tspo*$^{-/-}$ bone marrow, expression of *Alad* significantly increased after ALA treatment; this trend was not observed in *Tspo*$^{fl/fl}$ bone marrow. Mean baseline expression of *Cpox* was higher but not statistically different between *Tspo*$^{fl/fl}$ and *Tspo*$^{-/-}$ bone marrow, but with ALA treatment *Cpox* significantly decreased in both *Tspo*$^{-/-}$ and *Tspo*$^{fl/fl}$ bone marrow. Expression of *Tspo2* showed a decreasing trend after ALA treatment in both *Tspo*$^{fl/fl}$ and *Tspo*$^{-/-}$ bone marrow but was not significant. Expression of *Tspo* was significantly up-regulated compared with baseline after ALA treatment in *Tspo*$^{fl/fl}$ bone marrow.

Tissue Heme Levels in Tspo$^{-/-}$ *Mice*—In analytical preparations from tissues, emission spectra for PPIX measurements were highly specific when compared with standards allowing for the precise quantification of heme (Fig. 3*A*). Baseline heme

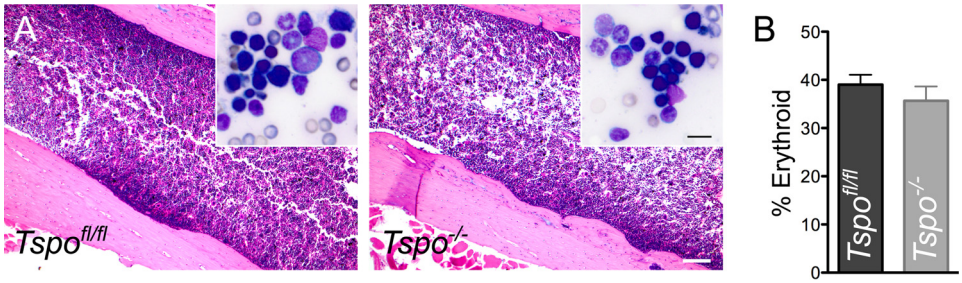

FIGURE 1. **Bone marrow histology and evaluation of erythroid cells.** *A*, sections of *Tspo*$^{fl/fl}$ and *Tspo*$^{-/-}$ mice femur bone showing the marrow. Histological evaluation of the marrow showed no difference in overall hematopoietic cellularity. *Scale bar*, 200 μm. *Inset*, bone marrow cytology; there was no difference in relative density of erythroid precursor cells. *Scale bar*, 15 μm. *B*, enumeration of erythroid cells showed no differences in the percentage of erythroid precursors between the two groups ($n = 3$/group).

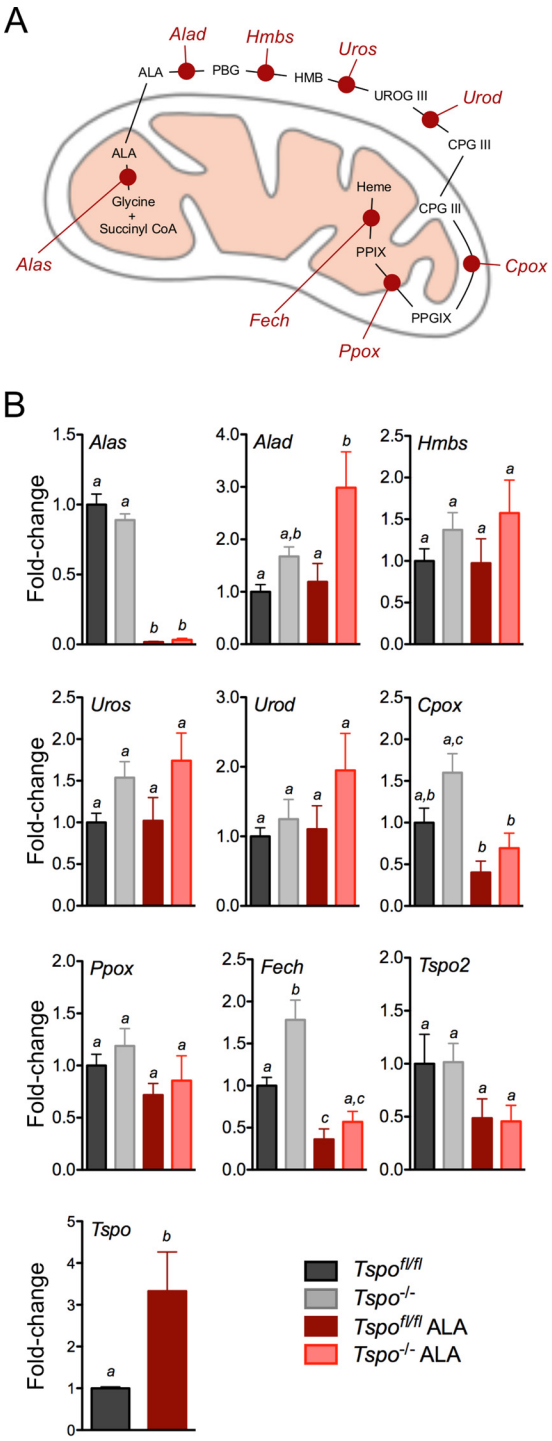

FIGURE 2. **Expression of genes involved in PPIX synthesis in *Tspo*$^{-/-}$ bone marrow.** *A*, schematic showing the different enzymatic steps involved in the conversion of ALA to PPIX and heme. The enzymes were ALA synthase (*Alas*), ALA dehydratase (*Alad*), hydroxymethyl bilane synthase (*Hmbs*), uroporphyrinogen III synthase (*Uros*), uroporphyrinogen decarboxylase (*Urod*), coproporphyrinogen oxidase (*Cpox*), protoporphyrinogen oxidase (*Ppox*), and ferrochelatase (*Fech*). The intermediates were porphobilinogen (*PBG*), hydroxymethyl bilane (*HMB*), uroporphyrinogen III (*UROG III*), coproporphyrinogen III (*CPG III*), and protoporphyrinogen IX (PPGIX). *B*, expression levels of transcripts coding enzymes involved in the conversion of ALA to PPIX in *Tspo*$^{fl/fl}$ and *Tspo*$^{-/-}$ bone marrow at both baseline and after treatment with ALA. *a*, *b*, and *c* indicate $p < 0.05$ ($n = 6$/group).

levels were not different between *Tspo*$^{fl/fl}$ and *Tspo*$^{-/-}$ livers and spleens (Fig. 3, *B* and *C*). However, heme levels were modestly higher but significant in bone marrow from *Tspo*$^{-/-}$ mice compared with *Tspo*$^{fl/fl}$ cohorts (Fig. 3*D*).

Systemic Conversion of ALA to PPIX in Tspo$^{-/-}$ *Mice*—Baseline PPIX concentrations in plasma, and tissue lysates (bone marrow, livers and spleens) were not different between *Tspo*$^{fl/fl}$ and *Tspo*$^{-/-}$ mice (Fig. 4). After ALA administration, increases in PPIX levels at 1, 4, and 8 h were similar in both *Tspo*$^{fl/fl}$ and *Tspo*$^{-/-}$ mice in plasma and all tissues.

TSPO Deficiency Does Not Affect PPIX Uptake and Localization—When *Tspo*$^{fl/fl}$ and *Tspo*$^{-/-}$ fibroblasts were treated with PPIX, the extent of PPIX localization to the mitochondria computed as overlap with MitoTracker® Green fluorescence was identical between the two genotypes (Fig. 5, *A*–*C*). Treatments of *Tspo*$^{fl/fl}$ and *Tspo*$^{-/-}$ fibroblasts with increasing concentrations of PPIX showed dose-dependent increases in intracellular fluorescence that were not different between the two genotypes (Fig. 5*D*). PPIX uptake by fibroblasts approached saturation at 1 μM PPIX treatment, with no difference observed when treatment was increased to 1.5 μM PPIX (Fig. 5*D*).

TSPO Deficiency Does Not Affect Porphyrin-mediated Phototoxicity—Without PPIX treatment, exposure of both *Tspo*$^{fl/fl}$ and *Tspo*$^{-/-}$ fibroblasts to light at 450 ± 60-nm wavelengths with increasing energies (160, 240, and 320 mJ) did not induce phototoxicity and cell death (Fig. 6). When these *Tspo*$^{fl/fl}$ and *Tspo*$^{-/-}$ fibroblasts were treated with PPIX, they displayed different levels of cell death that increased with both increasing concentration of PPIX and increasing energy of light (up to 95% cell death was observed with 1.5 μM of PPIX treatment and 320 mJ light energy). However, no significant differences in PPIX-mediated phototoxic cell death were observed between *Tspo*$^{fl/fl}$ and *Tspo*$^{-/-}$ fibroblasts (Fig. 6).

Bioconversion of ALA to PPIX Is Not Changed in Tspo$^{-/-}$ *Fibroblasts*—Baseline PPIX concentration in *Tspo*$^{fl/fl}$ and *Tspo*$^{-/-}$ fibroblast lysates were not different (Fig. 7*A*). After ALA treatment, PPIX concentrations in fibroblast lysates showed a significant increase with no statistical difference between the two genotypes (Fig. 7*A*). Expression of genes involved in PPIX biosynthesis indicated some differences between *Tspo*$^{fl/fl}$ and *Tspo*$^{-/-}$ fibroblasts (Fig. 7*B*). Baseline expression of *Alas*, *Hmbs*, *Urod*, *Cpox*, *Ppox*, and *Fech* were significantly lower in *Tspo*$^{-/-}$ compared with *Tspo*$^{fl/fl}$ fibroblasts; baseline expression of *Alad* and *Uros* was not different between the two genotypes. After ALA treatment, expression of *Alas*, *Alad*, *Hmbs*, and *Cpox* was not different between the two genotypes; expression of *Uros*, *Urod*, *Ppox*, and *Fech* was significantly lower in *Tspo*$^{-/-}$ compared with *Tspo*$^{fl/fl}$ fibroblasts. Expression of *Tspo* did not show any changes with ALA treatment in *Tspo*$^{fl/fl}$ fibroblasts. *Tspo2* expression was not detected in *Tspo*$^{fl/fl}$ and *Tspo*$^{-/-}$ fibroblasts at both baseline and after treatment with ALA (not shown).

Bioconversion of ALA to PPIX Is Not Changed in MA-10: Tspo$^{\Delta/\Delta}$ *Cells*—Baseline PPIX concentration in MA-10 cell lysates showed a modest but significantly lower level in MA-10: *Tspo*$^{\Delta/\Delta}$ cells compared with MA-10 cells (Fig. 8*A*). After ALA treatment, PPIX concentrations in cell lysates showed a significant increase with no difference between MA-10:*Tspo*$^{\Delta/\Delta}$ cells

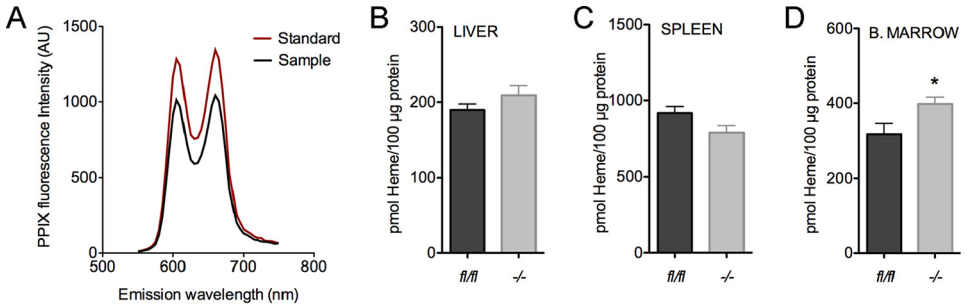

FIGURE 3. **Heme levels in tissues from *Tspo*$^{-/-}$ mice.** *A*, PPIX standard and a representative analytical spleen sample showing the emission spectrum of PPIX with excitation at 400 nm; two emission maximums at 605 and 660 nm specific for PPIX are observed in both standard and prepared sample. *B–D*, normalized baseline heme levels in tissues (liver, spleen, and bone marrow) from *Tspo*$^{fl/fl}$ and *Tspo*$^{-/-}$ mice. *, $p < 0.05$ ($n = 6$/group).

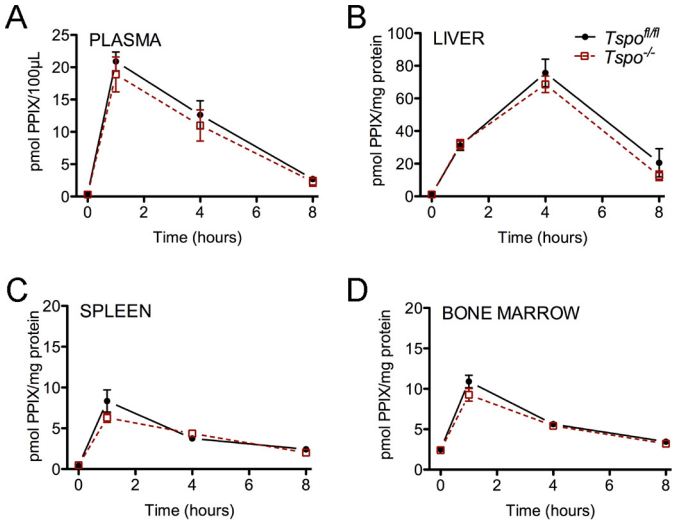

FIGURE 4. **PPIX levels in plasma and tissues from *Tspo*$^{-/-}$ mice.** Panels show normalized PPIX fluorescence in blood plasma (*A*), liver (*B*), spleen (*C*), and bone marrow (*D*), at baseline and at 1, 4, and 8 h after administration of ALA ($n = 6–8$/group).

and MA-10 cells (Fig. 8*A*). Expression of genes involved in PPIX biosynthesis indicated some differences between MA-10: *Tspo*$^{\Delta/\Delta}$ cells and MA-10 cells (Fig. 8*B*). Baseline expression of *Alad*, *Uros*, and *Urod* were significantly higher in MA-10: *Tspo*$^{\Delta/\Delta}$ cells compared with MA-10 cells, and these differences did not change after ALA treatment. Baseline expression of *Alas* was not different between MA-10:*Tspo*$^{\Delta/\Delta}$ cells and MA-10 cells, but expression significantly decreased upon ALA treatment in both genotypes. Baseline expression of *Hmbs*, *Cpox*, and *Ppox* was not different between MA-10:*Tspo*$^{\Delta/\Delta}$ cells and MA-10 cells, but a significant increase in expression was observed after ALA treatment only in MA-10:*Tspo*$^{\Delta/\Delta}$ cells compared with MA-10 cells. Baseline *Fech* expression was significantly decreased in MA-10:*Tspo*$^{\Delta/\Delta}$ cells compared with MA-10 cells; this difference was also seen after ALA treatment. Expression of *Tspo* showed a modest but significant decrease with ALA treatment in MA-10 cells. *Tspo2* expression was not observed in MA-10 cells and MA-10:*Tspo*$^{\Delta/\Delta}$ cells at both baseline and after treatment with ALA (not shown).

TSPO Expression Does Not Correlate to PPIX Production by Colon Cancer Cells—In comparing fibroblasts and MA-10 cells with different human colon cancer cell lines, TSPO expression was highest in MA-10 cells and weakest in fibroblasts; among the colon cancer cell lines, DLD1 > HT29 > HCT116≥LOVO (Fig. 9*A*). Expression of IDH2, used as an indirect measure of mitochondrial mass in the different colon cancer lines, showed a range of differences between the cell lines, suggesting varied mitochondrial masses; relative expression of ACTB was also not perfectly consistent for baseline normalization between the cell lines (Fig. 9*A*). PPIX synthesis after ALA treatment in the colon cancer cell lines showed levels decreasing in order from HT29 > HCT116 > DLD1 > LOVO cells (Fig. 9*B*). In LOVO cells, we did not observe enhanced PPIX production after ALA treatment. These observations support the results seen in MA-10 cells, suggesting that the efficacy of PPIX synthesis after ALA treatment is not related to TSPO expression in colon cancer cells.

Exogenous TSPO2 Expression Does Not Change ALA to PPIX Bioconversion in Fibroblasts—There was no expression of *Tspo2* observed in fibroblasts and MA-10 cells (Fig. 10*A*). Exogenous adenoviral *Tspo2* expression in *Tspo*$^{fl/fl}$ and *Tspo*$^{-/-}$ fibroblasts resulted in ~8-fold higher expression levels compared with endogenous expression observed in the bone marrow. PPIX synthesis before and after ALA treatment was not different between *Tspo*$^{fl/fl}$ and *Tspo*$^{-/-}$ fibroblasts after exogenous expression of *Tspo2* (Fig. 10*B*). In control *tdTomato* expression, ALA treatment showed a modest but significant increase in PPIX levels in *Tspo*$^{-/-}$ fibroblasts. However, this increase was not significantly different compared with *Tspo2* expressing *Tspo*$^{-/-}$ fibroblasts. These results suggest that TSPO2 expression does not have a positive or negative effect on PPIX production from ALA.

Mitochondrial Homeostasis Is Altered in Tspo$^{-/-}$ *Fibroblasts*—Comparing primary fibroblasts from *Tspo*$^{fl/fl}$ and *Tspo*$^{-/-}$ mice showed that baseline and maximal OCR were significantly lower with the loss of TSPO (Fig. 11*A*). However, the percentages of oxidative phosphorylation coupling efficiencies were unchanged in *Tspo*$^{-/-}$ compared with *Tspo*$^{fl/fl}$ fibroblasts (Fig. 11*B*), but absolute values were significantly lower in *Tspo*$^{-/-}$ fibroblasts (not shown). There was a decrease in calculated ATP production in *Tspo*$^{-/-}$ compared with *Tspo*$^{fl/fl}$ fibroblasts (Fig. 11*C*). Proton leak was also decreased in *Tspo*$^{-/-}$ compared with *Tspo*$^{fl/fl}$ fibroblasts (Fig. 11*D*). The spare respiratory capacity was significantly reduced in *Tspo*$^{-/-}$ compared with *Tspo*$^{fl/fl}$ fibroblasts (Fig. 11*E*). These findings suggest a significant shift in mitochondrial homeostasis in *Tspo*$^{-/-}$ fibroblasts that could affect multiple mitochondrial and cellular functions.

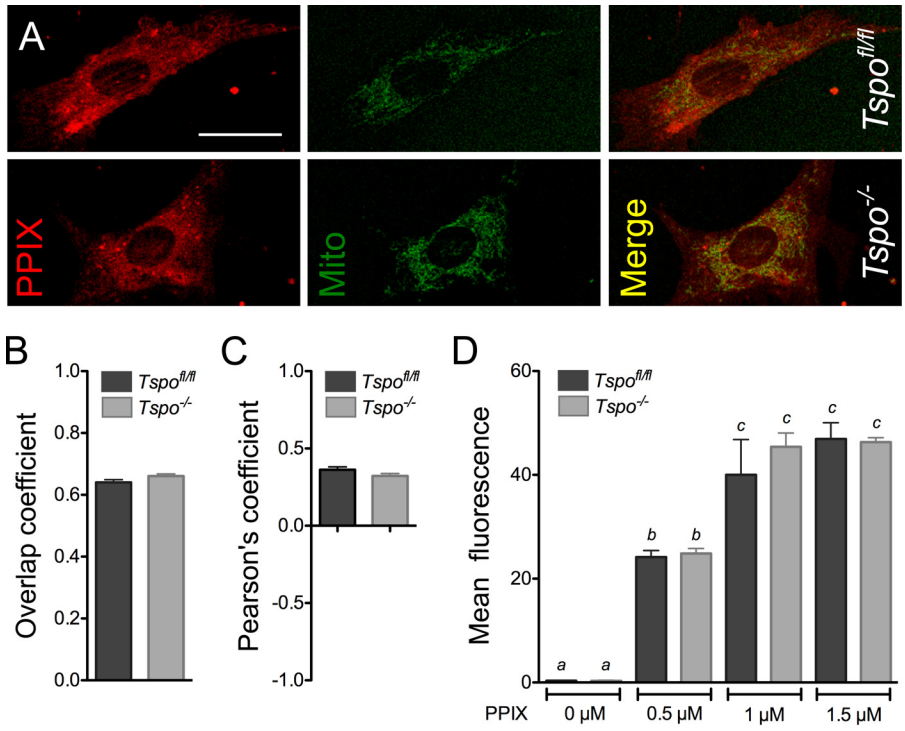

FIGURE 5. **PPIX uptake and localization in *Tspo*$^{fl/fl}$ and *Tspo*$^{-/-}$ fibroblasts.** *A*, PPIX fluorescence and MitoTracker® Green (*Mito*) colocalization in *Tspo*$^{fl/fl}$ and *Tspo*$^{-/-}$ fibroblasts. *Scale bar*, 50 μm. *B*, Mander's overlap coefficient for PPIX and MitoTracker® Green localization was not different between *Tspo*$^{fl/fl}$ and *Tspo*$^{-/-}$ fibroblasts. *C*, Pearson's coefficient for PPIX and MitoTracker® Green localization was not different between *Tspo*$^{fl/fl}$ and *Tspo*$^{-/-}$ fibroblasts. *D*, PPIX uptake by fibroblasts after treatment with increasing concentrations of PPIX (0, 0.5, 1.0, or 1.5 μM) for 4 h was not different between *Tspo*$^{fl/fl}$ and *Tspo*$^{-/-}$ cells. Mean fluorescence intensity for PPIX was measured by flow cytometry ($n = 6$ independent primary cultures/group).

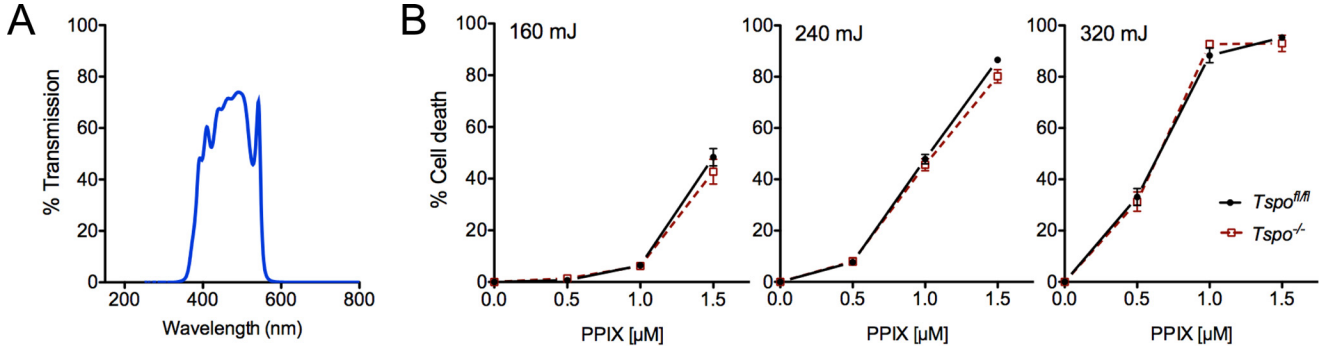

FIGURE 6. **Porphyrin-mediated phototoxicity in *Tspo*$^{fl/fl}$ and *Tspo*$^{-/-}$ fibroblasts.** *A*, spectrum of band pass filter used for photoexcitation allowed transmission of light 450 ± 60 nm. *B*, photoexcitation-induced cell death was not different between *Tspo*$^{fl/fl}$ and *Tspo*$^{-/-}$ after treatment with increasing concentrations of PPIX (0, 0.5, 1.0, or 1.5 μM) and subsequent exposure to increasing energies of light (160, 240, or 320 mJ; $n = 6$ independent primary cultures/group).

Mitochondrial Membrane Potential Is Decreased in Tspo$^{-/-}$ *Fibroblasts*—Assessment of ΔΨm showed that *Tspo*$^{-/-}$ fibroblasts had significantly lower baseline values compared with *Tspo*$^{fl/fl}$ fibroblasts, and this difference was increased after inhibition of ATP synthase by oligomycin and completely dissipated as expected after FCCP in both genotypes (Fig. 12, *A* and *B*). Given the scale of these changes as a result of TSPO deletion, we verified that mitochondrial volume and mass were not different between *Tspo*$^{-/-}$ and *Tspo*$^{fl/fl}$ fibroblasts (Fig. 12, *C–E*). Differences observed in *Tspo*$^{-/-}$ fibroblasts corroborate that loss of TSPO impacts mitochondrial homeostasis in primary cells.

PK11195 Does Not Affect ALA to PPIX Bioconversion but Has Off Target Effects Affecting ΔΨ*m*—Treatment with PK11195 [1 μM, the concentration used in the zebrafish study (24)], did not affect PPIX production after ALA treatment in both *Tspo*$^{fl/fl}$ and *Tspo*$^{-/-}$ fibroblasts (Fig. 13*A*). However, this same concentration of PK11195 significantly decreased ΔΨm in both *Tspo*$^{fl/fl}$ and *Tspo*$^{-/-}$ fibroblasts (Fig. 13*B*), indicating that PK11195 treatment can result in off target effects at this concentration. Baseline values for ΔΨm measured using flow cytometry also showed a significantly lower ΔΨm in *Tspo*$^{-/-}$ fibroblasts compared with *Tspo*$^{fl/fl}$ fibroblasts (Fig. 13*B*), consistent with the microscopic quantitation (Fig. 12*A* and *B*).

Discussion

Based on its conserved PPIX binding property (17), it was proposed that the ancestral role for TSPO could be enzyme catalysis of porphyrins, albeit only in the presence of light (46). Purified TSPO protein from *Chlorobium tepidum* (*Ct*TSPO)

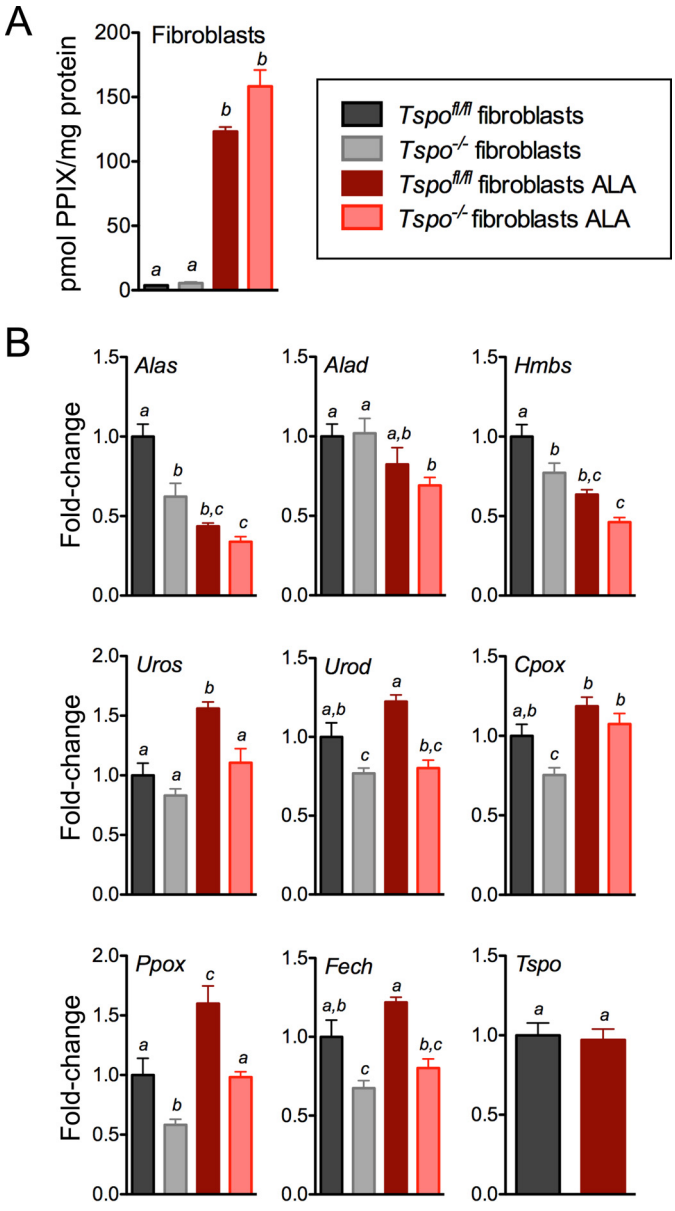

FIGURE 7. **PPIX synthesis from ALA in *Tspo*$^{fl/fl}$ and *Tspo*$^{-/-}$ fibroblasts.** *A*, PPIX concentration in *Tspo*$^{fl/fl}$ and *Tspo*$^{-/-}$ fibroblast cell lysates before and after treatment with ALA. *a* and *b* indicate $p < 0.05$ ($n = 3$/group). *B*, expression levels of transcripts coding enzymes involved in the conversion of ALA to PPIX in *Tspo*$^{fl/fl}$ and *Tspo*$^{-/-}$ fibroblasts at both baseline and after treatment with ALA. *a*, *b*, and *c* indicate $p < 0.05$ ($n = 6$ independent primary cultures/group).

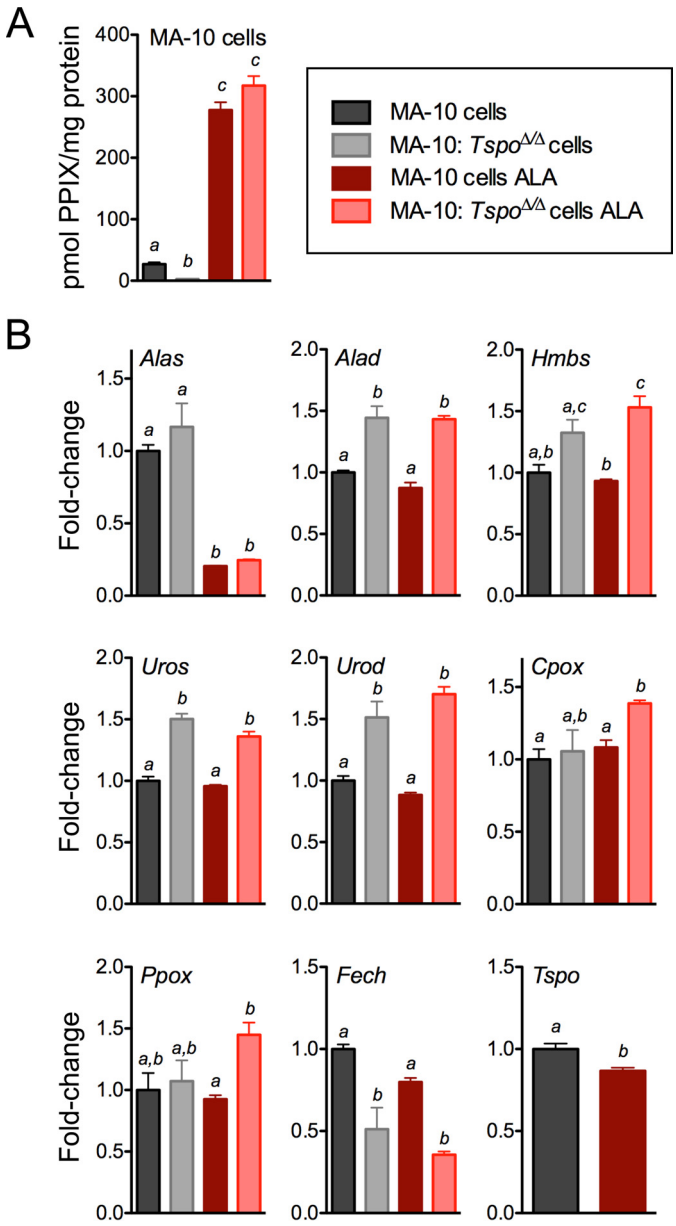

FIGURE 8. **PPIX synthesis from ALA in MA-10 cells and MA-10:*Tspo*$^{\Delta/\Delta}$ cells.** *A*, PPIX concentration in MA-10 cells and MA-10:*Tspo*$^{\Delta/\Delta}$ cell lysates before and after treatment with ALA. *a*, *b*, and *c* indicate $p < 0.05$ ($n = 3$/group). *B*, expression levels of transcripts coding enzymes involved in the conversion of ALA to PPIX in MA-10 cells and MA-10:*Tspo*$^{\Delta/\Delta}$ cells at both baseline and after treatment with ALA. *a*, *b*, and *c* indicate $p < 0.05$ ($n = 3$/group).

and *B. cereus* (*Bc*TSPO) indicated a property of photo-oxidative PPIX degradation (22, 46). In contrast, chordate TSPO (fish, birds, and mammals) has been suggested to be important for PPIX transport and heme biosynthesis (24, 25, 28, 47). The PPIX binding property of TSPO was also considered the basis of ALA-based PDT for cancers (38, 39, 48). Diverging from these conclusions, results in this manuscript suggest that TSPO does not have a physiological effect on PPIX metabolism and may not be involved in PDT.

Deficiency of TSPO did not affect heme synthesis and erythropoiesis in mice, suggesting an evolutionary shift distinct from its hematopoietic function reported in zebrafish (49). Bone marrow, the primary site of erythropoiesis, also expresses the TSPO paralog TSPO2 that can be found only in birds and mammals (49). TSPO2 has 35% homology to TSPO and is almost exclusively localized to the bone marrow (49). However, TSPO2 localization to the endoplasmic reticulum (49) suggests that it may not be involved in a mitochondrial function that is redundant to TSPO. Fibroblasts and MA-10 cells do not express TSPO2. Moreover, we confirmed that TSPO2 does not affect PPIX synthesis using adenovirus-induced *Tspo2* expression in fibroblasts, ruling out the possibility of functional redundancy. In support, expression of the heme biosynthetic gene *Fech* showed a compensatory baseline increase in expression in *Tspo*$^{-/-}$ bone marrow, suggesting that TSPO deletion

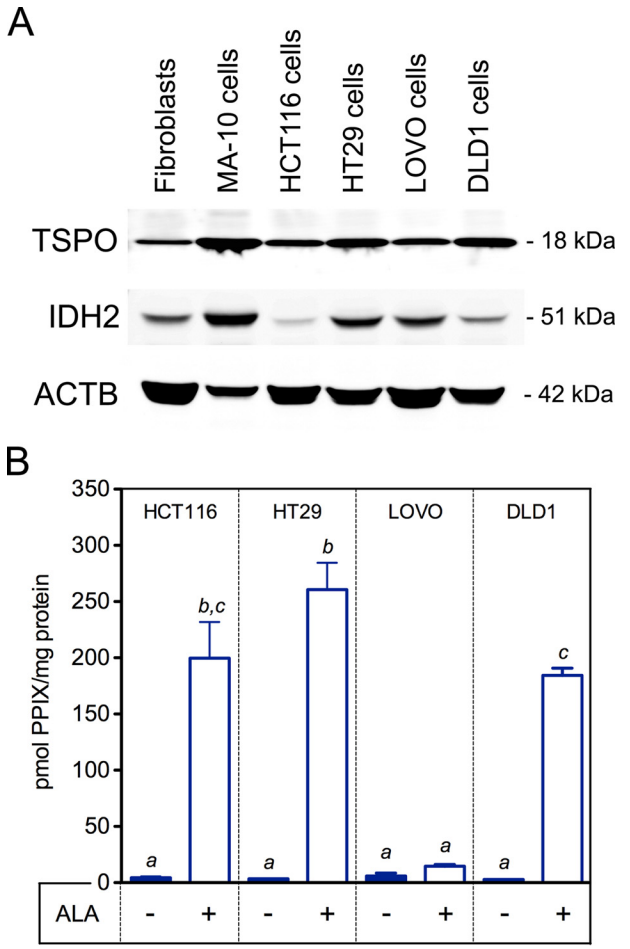

FIGURE 9. **TSPO expression levels and PPIX synthesis from ALA in colon cancer cells.** *A*, expression levels of TSPO and mitochondrial protein IDH2 in relation to ACTB in primary *Tspo*$^{fl/fl}$ fibroblasts, MA-10 Leydig cells, and four different colon cancer cell lines (HCT116, HT29, LOVO, and DLD1 cells). Equal total protein (50 μg) was loaded to generate this representative Western blot. *B*, PPIX concentration in cell lysates before and after treatment with ALA in HCT116, HT29, LOVO, and DLD1 colon cancer cell lines. *a*, *b*, and *c* indicate $p < 0.05$ ($n = 3$/group).

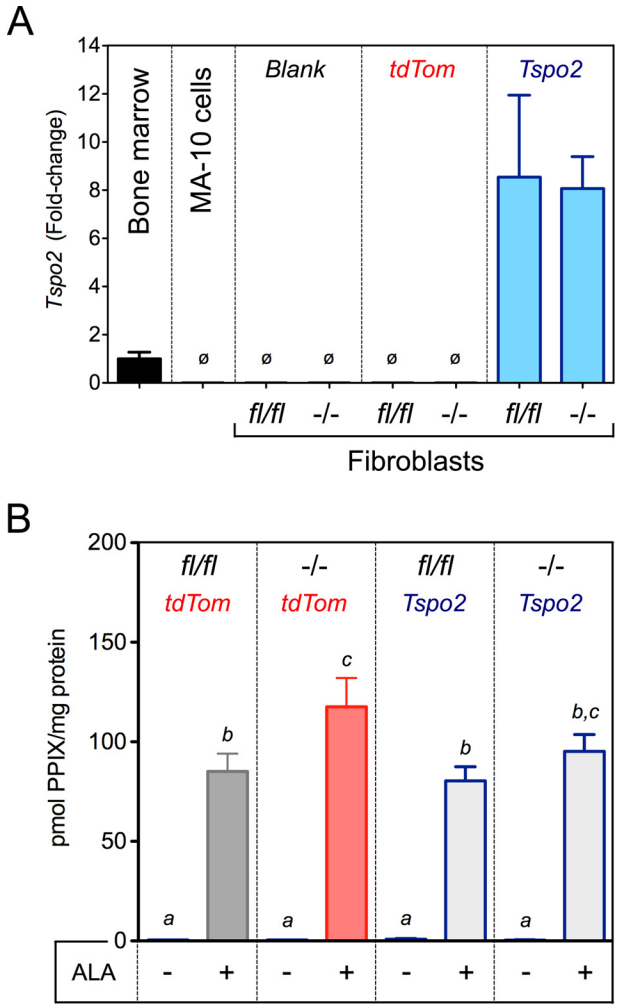

FIGURE 10. **Effect of TSPO2 expression on PPIX synthesis from ALA.** *A*, *Tspo2* gene expression normalized to endogenous expression in the bone marrow. Expression of *Tspo2* was not observed (ø) in MA-10 cells and fibroblasts (*blank*). Specific ~8-fold expression of *Tspo2* was induced by adenoviral expression in *Tspo*$^{fl/fl}$ and *Tspo*$^{-/-}$ fibroblasts. Adenovirus expressing *tdTomato* (*tdTom*) was examined as a negative control. *B*, PPIX concentration in *Tspo*$^{fl/fl}$ and *Tspo*$^{-/-}$ fibroblast lysates after induced expression of *tdTom* or *Tspo2*, before and after treatment with ALA. *a*, *b*, and *c* indicate $p < 0.05$ ($n = 3$/group).

did induce a shift in mitochondrial homeostasis. However, this shift in homeostasis toward increased heme synthesis did not alter physiological hemoglobin concentration measured in circulation. Moreover, when *Tspo*$^{-/-}$ mice were treated with ALA, there were no differences in maximal PPIX production in plasma, liver, spleen, and bone marrow. Although *Tspo* up-regulation was observed after ALA treatment in *Tspo*$^{fl/fl}$ bone marrow (functionally akin to previous reports of *Tspo* up-regulation during erythroid differentiation (28)), we infer that this is unrelated to PPIX biosynthesis or scavenging, because *Tspo*$^{-/-}$ mice had no differences in PPIX production. It is possible that administration of ALA promotes erythroid differentiation in the bone marrow, as observed in the widely used *in vitro* K562 erythroid differentiation model (50–52). A *Tspo* up-regulation response as reported in erythroid cells was not observed in fibroblasts or MA-10 cells, also suggesting that this is specific for the bone marrow.

To examine PPIX uptake and porphyrin-mediated phototoxicity in a system that expresses TSPO (but not TSPO2), we used primary fibroblasts as a model (53) to examine mechanisms. We found that TSPO deficiency did not affect the extent of PPIX association with the mitochondria and the level of uptake by fibroblasts. Moreover, PPIX-mediated phototoxic cell death was not different between *Tspo*$^{fl/fl}$ and *Tspo*$^{-/-}$ fibroblasts. Although these observations were rather unexpected given that previous studies reported the contrary in other model systems (12, 30, 54), they corroborated a recent report demonstrating that PPIX accumulation was not different in between *Tspo*$^{fl/fl}$ and *Tspo*$^{-/-}$ mitochondria isolated from the liver (16).

Early studies have established that CPOX is present in the mitochondrial intermembrane space and that coproporphyrinogen III needs to cross the outer mitochondrial membrane to gain access to this enzyme (55). Although weaker than its affinity for PPIX, TSPO was demonstrated to bind coproporphyrinogen III (28). Because TSPO-binding chemicals appeared to block the conversion of coproporphyrino-

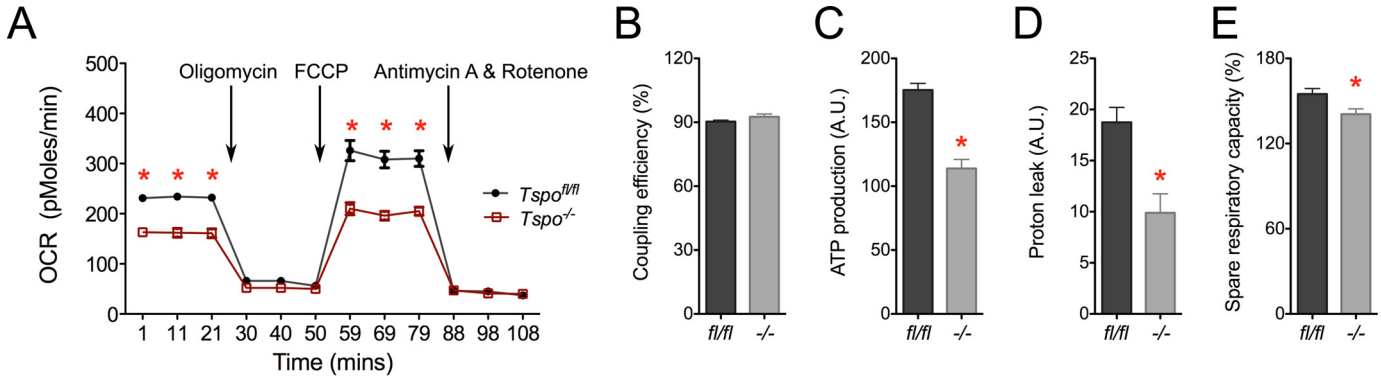

FIGURE 11. **Analysis of mitochondrial bioenergetics in *Tspo*$^{fl/fl}$ and *Tspo*$^{-/-}$ fibroblasts.** *A*, baseline OCR and maximal OCR after addition of the protonophore FCCP was significantly lower in *Tspo*$^{-/-}$ compared with *Tspo*$^{fl/fl}$ fibroblasts. OCR declined upon blocking ATP synthase activity using oligomycin or inhibiting electron transport chain using antimycin A and rotenone, but they were not significantly different between the two genotypes. *B*, mitochondrial coupling efficiency was not different between *Tspo*$^{fl/fl}$ and *Tspo*$^{-/-}$ fibroblasts. *C*, mitochondrial ATP production was significantly lower in *Tspo*$^{-/-}$ compared with *Tspo*$^{fl/fl}$ fibroblasts. *D*, proton leak was significantly lower in *Tspo*$^{-/-}$ compared with *Tspo*$^{fl/fl}$ fibroblasts. *E*, spare respiratory capacity was significantly lower in *Tspo*$^{-/-}$ compared with *Tspo*$^{fl/fl}$ fibroblasts. *, $p < 0.05$ ($n = 5$–7 independent primary cultures).

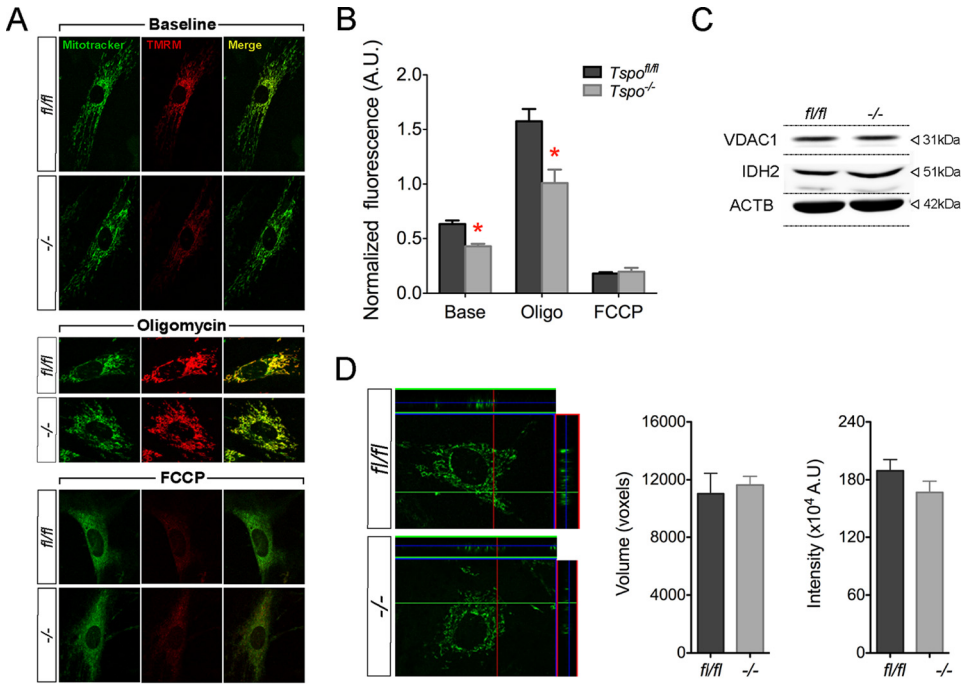

FIGURE 12. **Analysis of mitochondrial membrane potential ($\Delta\psi$m) in *Tspo*$^{fl/fl}$ and *Tspo*$^{-/-}$ fibroblasts.** *A*, representative images of *Tspo*$^{fl/fl}$ and *Tspo*$^{-/-}$ fibroblasts stained with TMRM and MitoTracker® Green from experiments measuring $\Delta\psi$m, showing baseline fluorescence, after treatment with oligomycin, and FCCP. *B*, normalized TMRM/MitoTracker® Green fluorescence intensity comparison between *Tspo*$^{fl/fl}$ and *Tspo*$^{-/-}$ fibroblasts showed significantly decreased $\Delta\psi$m at baseline and after oligomycin treatment. *, $p < 0.05$ ($n = 150$ cells/group). *C*, expression of mitochondrial proteins VDAC1 and IDH2 were not different between *Tspo*$^{fl/fl}$ and *Tspo*$^{-/-}$ fibroblasts. *D*, representative z-stacks of MitoTracker® Green stained *Tspo*$^{fl/fl}$ and *Tspo*$^{-/-}$ fibroblasts used for calculating mitochondrial volume. Mitochondrial volume was not different between *Tspo*$^{fl/fl}$ and *Tspo*$^{-/-}$ fibroblasts. Mitochondrial mass as measured by MitoTracker® Green labeling intensity was also not different between *Tspo*$^{fl/fl}$ and *Tspo*$^{-/-}$ fibroblasts ($n = 150$ cells/group).

gen III to PPIX via intermediate protoporphyrinogen IX, a possible function for TSPO as a porphyrin transporter was proposed (29). In support, it was demonstrated that TSPO was directly involved in PPIX transport in an experiment using bacterial protoplasts expressing murine TSPO (47). In the present study, when we examined the ability of fibroblasts to synthesize PPIX from precursor ALA, we found no difference between *Tspo*$^{-/-}$ and *Tspo*$^{fl/fl}$ cells. The exact same experiment in MA-10 cells (that also do not express TSPO2 but express ~14-fold higher TSPO compared with fibroblasts) showed no difference between MA-10 and MA-10:*Tspo*$^{\Delta/\Delta}$ cells. These results agreed with our *in vivo* observations in *Tspo*$^{-/-}$ mice and confirmed that TSPO is not involved in PPIX biosynthesis.

Provided the prognostic significance proposed for TSPO expression in colon cancer (56) and evidence that TSPO density in cancers parallels their susceptibility to porphyrin-mediated phototoxicity (54), we examined TSPO and PPIX synthesis in cancer cells. Comparison of different human colon cancer cell lines showed that TSPO expression had no correlation with PPIX synthesis capability, similar to observations in fibroblasts and MA-10 cells. Therefore, earlier reports indicating that TSPO directs mitochondrial porphyrin transport as part of the biosynthetic machinery (29, 47) are not substantiated. Recent

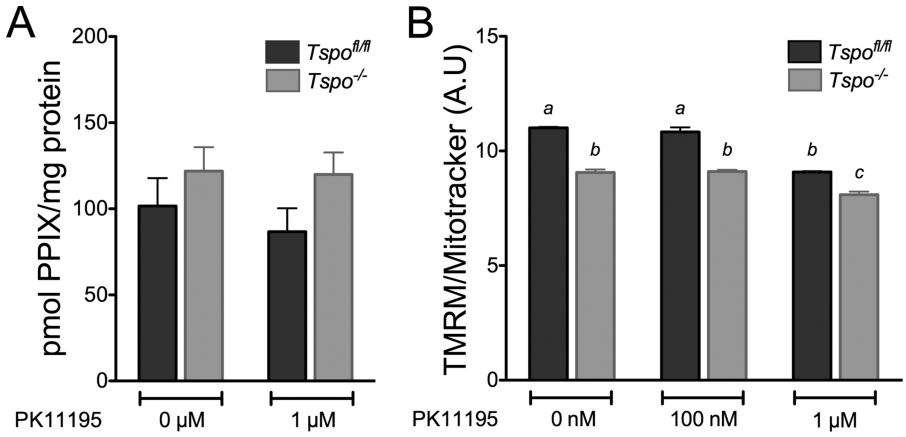

FIGURE 13. **Effect of PK11195 treatment on ALA to PPIX bioconversion and $\Delta\psi$m.** *A*, PPIX concentration in $Tspo^{fl/fl}$ and $Tspo^{-/-}$ fibroblast cell lysates after treatment with ALA in the presence of 0 (control) or 1 μM PK11195. Treatment with PK11195 did not have an effect PPIX production. *B*, normalized TMRM/MitoTracker® Green fluorescence intensity comparison between $Tspo^{fl/fl}$ and $Tspo^{-/-}$ fibroblasts after treatment with 0 (control) and 100 nM and 1 μM PK11195. Baseline $\Delta\psi$m was significantly lower in $Tspo^{-/-}$ compared with $Tspo^{fl/fl}$ fibroblasts. Treatment with PK11195 significantly decreased $\Delta\psi$m at 1 μM concentration in both $Tspo^{fl/fl}$ and $Tspo^{-/-}$ fibroblasts. *a* and *b* indicate $p < 0.05$ ($n = 4$ independent primary cultures/group).

identification of an essential porphyrin transporter ABCB6 (ATP-binding cassette, subfamily A (ABC1), member 6) at the outer mitochondrial membrane could explain the mechanism of mitochondrial porphyrin uptake and heme biosynthesis (57), without a role for TSPO in this process.

Although the PPIX binding property of TSPO is highly conserved and photo-oxidative degradation of PPIX could be considered an enzymatic function for TSPO, the physiological relevance of this slow and light-dependent activity in multicellular organisms appears unclear (58). Recent high resolution structural studies on *Mm*TSPO (*M. musculus*) (59), *Rs*TSPO (*R. sphaeroides*) (60), and *Bc*TSPO (22) highlight limited similarities between vertebrate (*Mm*TSPO) and the bacterial forms (*Rs*TSPO and *Bc*TSPO) with respect to PPIX binding residues, side chain interactions, and dimerization (58). In addition to the <30% identity, conserved residues that are organized on the outside of *Mm*TSPO are reversed in *Bc*TSPO and *Rs*TSPO. Moreover, *Mm*TSPO was found to be a monomer, *Rs*TSPO appears to form an obligate dimer, and *Bc*TSPO could also dimerize but does so with a distinct interface, suggesting evolutionary separations if this organization is indeed functionally important. Although the PPIX photo-oxidative degradation mediated by *Ct*TSPO and *Bc*TSPO are often discussed in broad terms, there is no functional evidence for this property in *Mm*TSPO. Experiments that used the vertebrate *Xt*TSPO (*Xenopus tropicalis*), and *Hs*TSPO (*H. sapiens*) A147T variant showed that the catalytic photo-oxidative degradation of PPIX is conserved in *Xt*TSPO but not in *Hs*TSPO (22). The photo-oxidative degradation property of the wild type *Hs*TSPO and *Mm*TSPO remains to be tested. Moreover, light-mediated reactions would be quite unusual for most tissues that express *Mm*TSPO or *Hs*TSPO. Therefore, results obtained for bacterial TSPO need to be extrapolated with caution, because they may not be conserved or relevant in higher vertebrates.

We find that TSPO deficiency significantly decreases OCR and $\Delta\Psi$m, indicating a distinct effect on core mitochondrial bioenergetics in fibroblasts that does not affect PPIX synthesis. This also indicates a potential shift in cellular energy homeostasis in $Tspo^{-/-}$ cells, which could affect multiple cellular events and responses. This shift in metabolic homeostasis could also explain gene expression differences in the heme biosynthetic pathway that were not only inconsistent between $Tspo^{-/-}$ bone marrow, fibroblasts, and MA-10 cells but also did not result in changes to PPIX production. In $Tspo^{-/-}$ primary microglia, a similar decrease in mitochondrial OCR was reported (10). Deletion of TSPO in *Drosophila melanogaster* ($dTspo^{-/-}$) also resulted in a decrease in mitochondrial OCR and oxidative phosphorylation complex activities (61). However, OCR changes were not observed in $Tspo^{-/-}$ mitochondria isolated from murine hepatocytes (16), suggesting that cell type-specific bioenergetics and other properties affected by the presence/absence or level of TSPO expression could influence observations.

Treatment of fibroblasts with PK11195 did not affect ALA to PPIX bioconversion. However, use of PK11195 decreased $\Delta\Psi$m in both $Tspo^{fl/fl}$ and $Tspo^{-/-}$ cells, suggesting that at least part of the effects observed using this agent is not mediated by TSPO. This observation indicates that some of the actions of PK11195 and other TSPO-binding drugs that have been linked to several seemingly disparate functions, without a physiological explanation (reviewed in Ref. 3 and 4), may be due to off target effects. Early studies that utilized TSPO-binding drugs, PK11195 and Ro5-4864 (4′-chlorodiazepam) demonstrated that they could induce a dose-dependent decrease in OCR (62) and inhibit mitochondrial respiratory control (63), similar to that observed in $Tspo^{-/-}$ cells. However, given our results using PK11195 in $Tspo^{-/-}$ cells, it is clear that specificity of TSPO binding and off target effects may preclude the ability to interpret results from pharmacological studies.

In conclusion, our results suggest that despite its reported PPIX binding property, *Mm*TSPO does not have an effect on erythropoiesis, heme biosynthesis, bioconversion of ALA to PPIX, or in porphyrin-mediated phototoxic cell death. Because TSPO is highly expressed in a variety of cancers, the lack of functional definition for TSPO does not preclude it from being a target for localizing photosensitizing agents as in PDT. However, meaningful interpretation of pharmacological effects

observed when using TSPO-binding drugs requires careful consideration of the limitations.

Author Contributions—V. S. and A. H. Z. conceived and designed the project. A. H. Z. performed most experiments, analyzed data, and interpreted results. L. N. T. performed experiments on mitochondrial bioenergetics, C. M. optimized the method and supervised analysis of lysates for PPIX levels, M. P. S. processed and interpreted bone marrow histology, V. V. P. built the Tspo2 adenoviral vector, K. M. supervised *in vivo* ALA to PPIX bioconversion experiments, and R. C. helped optimize and supervised mitochondrial membrane potential experiments. A. H. Z. and V. S. organized the figures and prepared the manuscript.

Acknowledgments—We thank the Diagnostic Center for Population and Animal Health at Michigan State University for hematology analysis, Dr. Rebecca M. Williams and Dr. Warren R. Zipfel for providing technical help with implementing the phototoxic cell death experiments, the Cornell Biotechnology Resource Center Imaging facility for providing the mercury light source, and Dr. Xiling Shen at Cornell University for sharing human colon cancer resources.

Note Added in Proof—In the original version of the manuscript that was published as a JBC Paper in Press, panels in Fig. 3 and Fig. 4 reporting heme and PPIX values in the y axis were in error due to a miscalculation of coordinates and scale. The correct y axis labels and values for heme and PPIX are now presented in the revised Fig. 3 and Fig. 4. This correction does not change interpretation of results or the conclusions.

References

1. Braestrup, C., and Squires, R. F. (1977) Specific benzodiazepine receptors in rat brain characterized by high-affinity (3H)diazepam binding. *Proc. Natl. Acad. Sci. U.S.A.* **74,** 3805–3809
2. Anholt, R. R., Pedersen, P. L., De Souza, E. B., and Snyder, S. H. (1986) The peripheral-type benzodiazepine receptor: localization to the mitochondrial outer membrane. *J. Biol. Chem.* **261,** 576–583
3. Gavish, M., Bachman, I., Shoukrun, R., Katz, Y., Veenman, L., Weisinger, G., and Weizman, A. (1999) Enigma of the peripheral benzodiazepine receptor. *Pharmacol. Rev.* **51,** 629–650
4. Selvaraj, V., and Stocco, D. M. (2015) The changing landscape in translocator protein (TSPO) function. *Trends Endocrinol. Metab.* **26,** 341–348
5. Papadopoulos, V., and Miller, W. L. (2012) Role of mitochondria in steroidogenesis. *Best Pract. Res. Clin. Endocrinol. Metab.* **26,** 771–790
6. Morohaku, K., Pelton, S. H., Daugherty, D. J., Butler, W. R., Deng, W., and Selvaraj, V. (2014) Translocator protein/peripheral benzodiazepine receptor is not required for steroid hormone biosynthesis. *Endocrinology* **155,** 89–97
7. Tu, L. N., Morohaku, K., Manna, P. R., Pelton, S. H., Butler, W. R., Stocco, D. M., and Selvaraj, V. (2014) Peripheral benzodiazepine receptor/translocator protein global knock-out mice are viable with no effects on steroid hormone biosynthesis. *J. Biol. Chem.* **289,** 27444–27454
8. Tu, L. N., Zhao, A. H., Stocco, D. M., and Selvaraj, V. (2015) PK11195 effect on steroidogenesis is not mediated through the translocator protein (TSPO). *Endocrinology* **156,** 1033–1039
9. Selvaraj, V., Stocco, D. M., and Tu, L. N. (2015) Translocator protein (TSPO) and steroidogenesis: a reappraisal. *Mol. Endocrinol.* **29,** 490–501
10. Banati, R. B., Middleton, R. J., Chan, R., Hatty, C. R., Kam, W. W., Quin, C., Graeber, M. B., Parmar, A., Zahra, D., Callaghan, P., Fok, S., Howell, N. R., Gregoire, M., Szabo, A., Pham, T., Davis, E., and Liu, G. J. (2014) Positron emission tomography and functional characterization of a complete PBR/TSPO knockout. *Nat. Commun.* **5,** 5452
11. McEnery, M. W., Snowman, A. M., Trifiletti, R. R., and Snyder, S. H. (1992) Isolation of the mitochondrial benzodiazepine receptor: association with the voltage-dependent anion channel and the adenine nucleotide carrier. *Proc. Natl. Acad. Sci. U.S.A.* **89,** 3170–3174
12. Pastorino, J. G., Simbula, G., Gilfor, E., Hoek, J. B., and Farber, J. L. (1994) Protoporphyrin IX, an endogenous ligand of the peripheral benzodiazepine receptor, potentiates induction of the mitochondrial permeability transition and the killing of cultured hepatocytes by rotenone. *J. Biol. Chem.* **269,** 31041–31046
13. Chelli, B., Falleni, A., Salvetti, F., Gremigni, V., Lucacchini, A., and Martini, C. (2001) Peripheral-type benzodiazepine receptor ligands: mitochondrial permeability transition induction in rat cardiac tissue. *Biochem Pharmacol* **61,** 695–705
14. Sileikyte, J., Petronilli, V., Zulian, A., Dabbeni-Sala, F., Tognon, G., Nikolov, P., Bernardi, P., and Ricchelli, F. (2011) Regulation of the inner membrane mitochondrial permeability transition by the outer membrane translocator protein (peripheral benzodiazepine receptor). *J. Biol. Chem.* **286,** 1046–1053
15. Giorgio, V., von Stockum, S., Antoniel, M., Fabbro, A., Fogolari, F., Forte, M., Glick, G. D., Petronilli, V., Zoratti, M., Szabó, I., Lippe, G., and Bernardi, P. (2013) Dimers of mitochondrial ATP synthase form the permeability transition pore. *Proc. Natl. Acad. Sci. U.S.A.* **110,** 5887–5892
16. Sileikyte, J., Blachly-Dyson, E., Sewell, R., Carpi, A., Menabò, R., Di Lisa, F., Ricchelli, F., Bernardi, P., and Forte, M. (2014) Regulation of the mitochondrial permeability transition pore by the outer membrane does not involve the peripheral benzodiazepine receptor (translocator protein of 18 kDa (TSPO)). *J. Biol. Chem.* **289,** 13769–13781
17. Verma, A., Nye, J. S., and Snyder, S. H. (1987) Porphyrins are endogenous ligands for the mitochondrial (peripheral-type) benzodiazepine receptor. *Proc. Natl. Acad. Sci. U.S.A.* **84,** 2256–2260
18. Yeliseev, A. A., and Kaplan, S. (1995) A sensory transducer homologous to the mammalian peripheral-type benzodiazepine receptor regulates photosynthetic membrane complex formation in Rhodobacter sphaeroides 2.4.1. *J. Biol. Chem.* **270,** 21167–21175
19. Frank, W., Baar, K. M., Qudeimat, E., Woriedh, M., Alawady, A., Ratnadewi, D., Gremillon, L., Grimm, B., and Reski, R. (2007) A mitochondrial protein homologous to the mammalian peripheral-type benzodiazepine receptor is essential for stress adaptation in plants. *Plant J.* **51,** 1004–1018
20. Yeliseev, A. A., Krueger, K. E., and Kaplan, S. (1997) A mammalian mitochondrial drug receptor functions as a bacterial "oxygen" sensor. *Proc. Natl. Acad. Sci. U.S.A.* **94,** 5101–5106
21. Yeliseev, A. A., and Kaplan, S. (1999) A novel mechanism for the regulation of photosynthesis gene expression by the TspO outer membrane protein of *Rhodobacter sphaeroides* 2.4.1. *J. Biol. Chem.* **274,** 21234–21243
22. Guo, Y., Kalathur, R. C., Liu, Q., Kloss, B., Bruni, R., Ginter, C., Kloppmann, E., Rost, B., and Hendrickson, W. A. (2015) Protein structure. Structure and activity of tryptophan-rich TSPO proteins. *Science* **347,** 551–555
23. Vanhee, C., Zapotoczny, G., Masquelier, D., Ghislain, M., and Batoko, H. (2011) The *Arabidopsis* multistress regulator TSPO is a heme binding membrane protein and a potential scavenger of porphyrins via an autophagy-dependent degradation mechanism. *Plant Cell* **23,** 785–805
24. Rampon, C., Bouzaffour, M., Ostuni, M. A., Dufourcq, P., Girard, C., Freyssinet, J. M., Lacapere, J. J., Schweizer-Groyer, G., and Vriz, S. (2009) Translocator protein (18 kDa) is involved in primitive erythropoiesis in zebrafish. *FASEB J.* **23,** 4181–4192
25. Nakazawa, F., Alev, C., Shin, M., Nakaya, Y., Jakt, L. M., and Sheng, G. (2009) PBRL, a putative peripheral benzodiazepine receptor, in primitive erythropoiesis. *Gene Expr. Patterns* **9,** 114–121
26. Clarke, G. D., and Ryan, P. J. (1980) Tranquillizers can block mitogenesis in 3T3 cells and induce differentiation in Friend cells. *Nature* **287,** 160–161
27. Wang, J. K., Morgan, J. I., and Spector, S. (1984) Differentiation of Friend erythroleukemia cells induced by benzodiazepines. *Proc. Natl. Acad. Sci. U.S.A.* **81,** 3770–3772
28. Taketani, S., Kohno, H., Okuda, M., Furukawa, T., and Tokunaga, R. (1994) Induction of peripheral-type benzodiazepine receptors during differentiation of mouse erythroleukemia cells. A possible involvement of these receptors in heme biosynthesis. *J. Biol. Chem.* **269,** 7527–7531
29. Taketani, S., Kohno, H., Furukawa, T., and Tokunaga, R. (1995) Involve-

ment of peripheral-type benzodiazepine receptors in the intracellular transport of heme and porphyrins. *J. Biochem.* **117,** 875–880
30. Zeno, S., Veenman, L., Katz, Y., Bode, J., Gavish, M., and Zaaroor, M. (2012) The 18 kDa mitochondrial translocator protein (TSPO) prevents accumulation of protoporphyrin IX. Involvement of reactive oxygen species (ROS). *Curr. Mol. Med.* **12,** 494–501
31. Batarseh, A., and Papadopoulos, V. (2010) Regulation of translocator protein 18 kDa (TSPO) expression in health and disease states. *Mol. Cell. Endocrinol.* **327,** 1–12
32. Austin, C. J., Kahlert, J., Kassiou, M., and Rendina, L. M. (2013) The translocator protein (TSPO): a novel target for cancer chemotherapy. *Int. J. Biochem. Cell Biol.* **45,** 1212–1216
33. Hardwick, M., Fertikh, D., Culty, M., Li, H., Vidic, B., and Papadopoulos, V. (1999) Peripheral-type benzodiazepine receptor (PBR) in human breast cancer: correlation of breast cancer cell aggressive phenotype with PBR expression, nuclear localization, and PBR-mediated cell proliferation and nuclear transport of cholesterol. *Cancer Res.* **59,** 831–842
34. Galiègue, S., Casellas, P., Kramar, A., Tinel, N., and Simony-Lafontaine, J. (2004) Immunohistochemical assessment of the peripheral benzodiazepine receptor in breast cancer and its relationship with survival. *Clin. Cancer Res.* **10,** 2058–2064
35. Maaser, K., Grabowski, P., Oezdem, Y., Krahn, A., Heine, B., Stein, H., Buhr, H., Zeitz, M., and Scherübl, H. (2005) Up-regulation of the peripheral benzodiazepine receptor during human colorectal carcinogenesis and tumor spread. *Clin. Cancer Res.* **11,** 1751–1756
36. Peng, Q., Warloe, T., Berg, K., Moan, J., Kongshaug, M., Giercksky, K. E., and Nesland, J. M. (1997) 5-Aminolevulinic acid-based photodynamic therapy: clinical research and future challenges. *Cancer* **79,** 2282–2308
37. Krieg, R. C., Messmann, H., Rauch, J., Seeger, S., and Knuechel, R. (2002) Metabolic characterization of tumor cell-specific protoporphyrin IX accumulation after exposure to 5-aminolevulinic acid in human colonic cells. *Photochem. Photobiol.* **76,** 518–525
38. Bisland, S. K., Goebel, E. A., Hassanali, N. S., Johnson, C., and Wilson, B. C. (2007) Increased expression of mitochondrial benzodiazepine receptors following low-level light treatment facilitates enhanced protoporphyrin IX production in glioma-derived cells *in vitro*. *Lasers Surg. Med.* **39,** 678–684
39. Furre, I. E., Shahzidi, S., Luksiene, Z., Møller, M. T., Borgen, E., Morgan, J., Tkacz-Stachowska, K., Nesland, J. M., and Peng, Q. (2005) Targeting PBR by hexaminolevulinate-mediated photodynamic therapy induces apoptosis through translocation of apoptosis-inducing factor in human leukemia cells. *Cancer Res.* **65,** 11051–11060
40. Morrison, G. R. (1965) Fluorometric microdetermination of heme protein. *Anal. Chem.* **37,** 1124–1126
41. Morohaku, K., Phuong, N. S., and Selvaraj, V. (2013) Developmental expression of translocator protein/peripheral benzodiazepine receptor in reproductive tissues. *PLoS One* **8,** e74509
42. Schneider, C. A., Rasband, W. S., and Eliceiri, K. W. (2012) NIH Image to ImageJ: 25 years of image analysis. *Nat. Methods* **9,** 671–675
43. Livak, K. J., and Schmittgen, T. D. (2001) Analysis of relative gene expression data using real-time quantitative PCR and the $2(-\Delta\Delta C(T))$ method. *Methods* **25,** 402–408
44. Luo, J., Deng, Z. L., Luo, X., Tang, N., Song, W. X., Chen, J., Sharff, K. A., Luu, H. H., Haydon, R. C., Kinzler, K. W., Vogelstein, B., and He, T. C. (2007) A protocol for rapid generation of recombinant adenoviruses using the AdEasy system. *Nat. Protoc.* **2,** 1236–1247
45. Ollion, J., Cochennec, J., Loll, F., Escudé, C., and Boudier, T. (2013) TANGO: a generic tool for high-throughput 3D image analysis for studying nuclear organization. *Bioinformatics* **29,** 1840–1841
46. Ginter, C., Kiburu, I., and Boudker, O. (2013) Chemical catalysis by the translocator protein (18 kDa). *Biochemistry* **52,** 3609–3611
47. Wendler, G., Lindemann, P., Lacapère, J. J., and Papadopoulos, V. (2003) Protoporphyrin IX binding and transport by recombinant mouse PBR. *Biochem. Biophys. Res. Commun.* **311,** 847–852
48. Ratcliffe, S. L., and Matthews, E. K. (1995) Modification of the photodynamic action of delta-aminolaevulinic acid (ALA) on rat pancreatoma cells by mitochondrial benzodiazepine receptor ligands. *Br. J. Cancer* **71,** 300–305
49. Fan, J., Rone, M. B., and Papadopoulos, V. (2009) Translocator protein 2 is involved in cholesterol redistribution during erythropoiesis. *J. Biol. Chem.* **284,** 30484–30497
50. Kawasaki, N., Morimoto, K., Tanimoto, T., and Hayakawa, T. (1996) Control of hemoglobin synthesis in erythroid differentiating K562 cells: I. role of iron in erythroid cell heme synthesis. *Arch. Biochem. Biophys.* **328,** 289–294
51. Taketani, S., Furukawa, T., and Furuyama, K. (2001) Expression of coproporphyrinogen oxidase and synthesis of hemoglobin in human erythroleukemia K562 cells. *Eur. J. Biochem.* **268,** 1705–1711
52. Chiabrando, D., Marro, S., Mercurio, S., Giorgi, C., Petrillo, S., Vinchi, F., Fiorito, V., Fagoonee, S., Camporeale, A., Turco, E., Merlo, G. R., Silengo, L., Altruda, F., Pinton, P., and Tolosano, E. (2012) The mitochondrial heme exporter FLVCR1b mediates erythroid differentiation. *J. Clin. Invest.* **122,** 4569–4579
53. Li, G., Szewczuk, M. R., Raptis, L., Johnson, J. G., Weagle, G. E., Pottier, R. H., and Kennedy, J. C. (1999) Rodent fibroblast model for studies of response of malignant cells to exogenous 5-aminolevulinic acid. *Br. J. Cancer* **80,** 676–684
54. Verma, A., Facchina, S. L., Hirsch, D. J., Song, S. Y., Dillahey, L. F., Williams, J. R., and Snyder, S. H. (1998) Photodynamic tumor therapy: mitochondrial benzodiazepine receptors as a therapeutic target. *Mol. Med.* **4,** 40–45
55. Elder, G. H., and Evans, J. O. (1978) Evidence that the coproporphyrinogen oxidase activity of rat liver is situated in the intermembrane space of mitochondria. *Biochem. J.* **172,** 345–347
56. Maaser, K., Grabowski, P., Sutter, A. P., Höpfner, M., Foss, H. D., Stein, H., Berger, G., Gavish, M., Zeitz, M., and Scherübl, H. (2002) Overexpression of the peripheral benzodiazepine receptor is a relevant prognostic factor in stage III colorectal cancer. *Clin. Cancer Res.* **8,** 3205–3209
57. Krishnamurthy, P. C., Du, G., Fukuda, Y., Sun, D., Sampath, J., Mercer, K. E., Wang, J., Sosa-Pineda, B., Murti, K. G., and Schuetz, J. D. (2006) Identification of a mammalian mitochondrial porphyrin transporter. *Nature* **443,** 586–589
58. Li, F., Liu, J., Garavito, R. M., and Ferguson-Miller, S. (2015) Evolving understanding of translocator protein 18kDa (TSPO). *Pharmacol. Res.* **99,** 404–409
59. Jaremko, L., Jaremko, M., Giller, K., Becker, S., and Zweckstetter, M. (2014) Structure of the mitochondrial translocator protein in complex with a diagnostic ligand. *Science* **343,** 1363–1366
60. Li, F., Liu, J., Zheng, Y., Garavito, R. M., and Ferguson-Miller, S. (2015) Protein structure: crystal structures of translocator protein (TSPO) and mutant mimic of a human polymorphism. *Science* **347,** 555–558
61. Lin, R., Angelin, A., Da Settimo, F., Martini, C., Taliani, S., Zhu, S., and Wallace, D. C. (2014) Genetic analysis of dTSPO, an outer mitochondrial membrane protein, reveals its functions in apoptosis, longevity, and Aβ42-induced neurodegeneration. *Aging Cell* **13,** 507–518
62. Larcher, J. C., Vayssiere, J. L., Le Marquer, F. J., Cordeau, L. R., Keane, P. E., Bachy, A., Gros, F., and Croizat, B. P. (1989) Effects of peripheral benzodiazepines upon the O2 consumption of neuroblastoma cells. *Eur. J. Pharmacol.* **161,** 197–202
63. Hirsch, J. D., Beyer, C. F., Malkowitz, L., Beer, B., and Blume, A. J. (1989) Mitochondrial benzodiazepine receptors mediate inhibition of mitochondrial respiratory control. *Mol. Pharmacol.* **35,** 157–163